

# RUPTURE HISTORY AND STRONG GROUND MOTION MODELING OF THE 1992 CAPE MENDOCINO EARTHQUAKE

Robert W. Graves

*Woodward-Clyde Federal Services, 566 El Dorado Street Suite 100, Pasadena, CA  
PH: (818) 449-7650 / FAX: (818) 449-3536  
e-mail: rwgrave0@wcc.com*

October 27, 1994

## **Abstract**

The 1992 Cape Mendocino earthquake occurred at the southern end of the Cascadia Subduction zone and is the first historic event with fault rupture that is consistent with large-scale convergence on the Cascadia plate interface. The mainshock was well recorded by strong motion stations in the epicentral region and these data provide us with a unique opportunity to study source and wave propagation characteristics specific to the Cascadia Subduction zone. Using these data, we have employed a forward modeling procedure to derive a heterogeneous-slip rupture model which produces synthetic ground motions that are in good agreement with the observed responses. Our preferred rupture model has a moment of  $3.0 \times 10^{26}$  dyne-cm, a strike of  $350^\circ$ , a dip of  $14^\circ$  to the northeast, a rake of  $105^\circ$ , a length along strike of 32 km, and a down-dip width of 32 km. We obtain a maximum slip value of nearly 8 meters, with most of the slip concentrated in a region near the hypocenter. To the north of the epicentral region, several strong motion recording stations are located atop the sediments of the Eel River basin. The basin recordings are richer in long period energy and exhibit much longer durations than nearby hard rock recordings. To investigate these effects, we have performed 3D elastic finite-difference calculations incorporating the structure of the Eel River basin and using the heterogeneous-slip rupture model derived by forward modeling. The numerical calculations demonstrate that the observed effects are related to the trapping and focusing of seismic energy within the basin sediments. Record sections of the seismograms indicate that surface waves are generated at the near-source margin of the basin, and then propagate northward across the basin with a slow apparent velocity, leading to the long durations which are observed at the basin sites. It appears that the direct S-wave observed at the basin sites is controlled primarily by the earthquake source, while the surface waves are most sensitive to the structure and geometry of the underlying basin.

## **Introduction**

The 1992 Cape Mendocino Earthquake occurred along the coast of northern California in the vicinity of the Mendocino Triple Junction and could possibly be the first subduction earthquake known to have occurred on the Cascadia plate interface in historical times (Figure 1). Teleseismic determinations of the mainshock focal mechanism along with the distribution of aftershocks indicate nearly pure thrust motion on a northerly striking fault plane, having a

shallow dip of  $14^\circ$  to the east (Oppenheimer et al., 1993). There is currently some debate as to whether this event occurred on the shallow plate interface or on a sub-parallel structure in the lower continental crust (eg., Wang and Rogers, 1994). However, the rupture mechanism and the observed static deformation are consistent with convergence at the plate boundary, and the resulting ground motions should therefore be representative of a subduction type event (Murray et al., 1994). Historically, this region of California has had a high rate of seismic activity, including the occurrence of several moderate to large events in recent years (Table 1). The 1992 event is one of the largest earthquakes to have occurred in this region and it was recorded by several strong motion accelerographs in the epicentral region. These strong motion data provide a unique opportunity to study source and wave propagation characteristics for subduction type events along the Cascadia Subduction Zone.

At long-periods ( $T > 1$  sec), the strong ground motions in the epicentral region of large earthquakes are controlled primarily by deterministic features of the earthquake source and seismic wave propagation. Recent studies have demonstrated the utility of synthetic seismogram modeling techniques to match the recorded data and develop heterogeneous-slip rupture models of past earthquakes (eg., Mendoza and Hartzell, 1988; Heaton, 1990; Wald et al., 1994). A major concern in studies of this type is the separation of earthquake source and wave propagation effects in the recorded data. Many times, earthquakes occur in regions of complicated geology and wave propagation through these variable geologic structures can significantly affect the observed strong ground motions, particularly at periods greater than 1 sec. For example, Vidale and Helmberger (1988) demonstrated that the long-period (1-10 sec) strong ground motions recorded in the Los Angeles region during the 1971 San Fernando earthquake were dominated by surface wave energy that was generated by seismic waves trapped within the San Fernando and Los Angeles basins. These surface waves were characterized by large amplitudes and long durations, and in order to adequately explain these types of phenomena, 2D and/or 3D models of the near-surface geology are required.

In the case of the Cape Mendocino event, we face a similar problem in separating source and wave propagation effects in the observed data. Strong motion recording sites at Petrolia (petr), Cape Mendocino (capm), and Bunker Hill (bunk) are all located on hard rock directly above the fault plane (Figure 1), and much of the waveform information in these records is related to the details of the earthquake source. Further to the north, several other strong motion recording stations are located atop the sediments of the Eel River basin (Figure 1). This structure is a southeast-northwest trending river valley with sediments reaching depths of about 3 km. The basin recordings (cent, fern, fort, frtn, lolt) are richer in long-period energy and exhibit much longer durations than the hard rock recordings, suggesting the presence of basin generated surface waves (Figure 2). In order to explain these data we have used a combination of numerical simulation and modeling techniques to derive a variable-slip rupture model of the event, and also investigate wave propagation effects related to the structure of the Eel River basin.

In the sections that follow, we first discuss the development of a suitable rupture model of the Cape Mendocino earthquake. The rupture model is derived using a forward modeling technique that is based on the simulation procedure of Hartzell and Heaton (1983), and is constrained primarily with the data from the three closest strong motion stations. Next, we analyze the data recorded at the Eel River basin sites. In order to model these data, we use a 3D finite-difference simulation technique that incorporates not only an appropriate finite-fault source

model, but also the laterally varying geology of the Eel River basin. Using this approach, we can identify and model the generation of surface wave energy within the basin structure, as well as account for the complexities of the earthquake source. As an application of this technique to model expected ground motions for future earthquakes in the Pacific Northwest, in the final section, we present some preliminary results of simulations that have been performed in the Puget Sound region for a hypothetical  $M_w$  8 subduction zone event. These simulation results demonstrate the strong influence of the shallow basin structure on ground motions in the period range of 1-5 sec near the city of Seattle.

## **Cape Mendocino Earthquake**

### *Strong Motion Data*

The ground motion data used in our analysis were recorded at USGS and CSMIP accelerograph stations located in the epicentral region of the earthquake (Figure 1). Since we are primarily interested in the deterministic features of the ground motions, we will restrict our analysis to recordings of ground velocity having periods of 1 sec or greater. The data from the CSMIP sites (capm, petr, fort) has been processed, integrated, and released in digital form (Darragh et al., 1992), while the data from the USGS sites (bunk, cent, fern, frtn, lolt) has only been released in analog form (USGS, 1992). Consequently, the USGS acceleration time histories have been hand digitized, filtered, and integrated to obtain velocity time histories. In addition, absolute timing is only available for the CSMIP stations (capm, petr, and fort). The band-pass filtered (0.14 - 1.0 Hz) velocity records are shown in Figure 2.

As mentioned above, the data for the Eel River basin sites (cent, fern, fort, frtn, lolt) appears to be richer in long period energy and shows longer durations than the data from the hard rock sites (bunk, capm, petr), indicating wave interactions with the structure of the basin. These effects become quite evident when the data is viewed along a profile extending to the north of the source region (Figure 3). In this figure, the data are plotted as a function of increasing epicentral distance. The closest site (bunk) is located on hard rock, and the remaining sites extend across the basin. A series of large amplitude later arrivals, with slow apparent velocity are clearly seen in the basin site recordings. Timing lines have been superimposed on this figure to help facilitate identification of these arrivals and it is evident that these later arriving waves did not originate at the source, but were generated near station cent, at the near-source margin of the basin. Before addressing the basin response effects observed at these more distant sites in greater detail, we will first concentrate on modeling the earthquake source using the data recorded at the three closest stations (bunk, capm, petr).

### *Variable-Slip Rupture Model*

Our approach here is to develop a variable-slip rupture model of the Cape Mendocino mainshock that is consistent with the teleseismic focal mechanism and aftershock distribution, and which also explains the strong motion data recorded in the epicentral region. Due to the limited amount of strong motion recordings available, it is impractical to perform a formal inversion of these data to obtain a fault rupture model. In light of this, we will employ a forward

modeling approach, in which synthetic ground motions are calculated for each of the sites based on a given rupture model. The rupture model is then adjusted in a trial and error procedure until an appropriate match is obtained between the calculated ground motions and the observed responses. The synthetic motions are computed using the simulation technique of Hartzell and Heaton (1983). In this technique, faulting is represented as slip on a planar surface that is discretized into a number of subfaults. The response at a given station can be determined as a linear sum of the weighted subfault contributions, each appropriately delayed in time to simulate fault rupture. Wave propagation effects are modeled by Green's functions computed for a flat-layered velocity model (Table 2) using a frequency-wavenumber (FK) integration technique (Saikia, 1993).

Based on the teleseismic focal mechanism and the distribution of aftershocks (see Oppenheimer et al., 1993), we have constrained our fault model to have a strike of  $350^\circ$ , a dip of  $14^\circ$  to the northwest, a rake of  $105^\circ$ , a length along strike of 32 km, a down-dip width of 32 km, and a depth to the top edge of the fault plane of 4.2 km. The midway point of the top edge is located at  $40.357^\circ$  N and  $124.494^\circ$  W. The surface projection of this fault area is shown by the shaded region in Figure 1. We have used the epicenter location listed in Table 1 and a moment of  $3.0 \times 10^{26}$  dyne-cm ( $M_w=7$ ). Given these constraints, our primary objective is to find the distribution of slip across the fault plane, which adequately explains the observed strong ground motions at stations bunk, capm, and petr.

The fault plane was divided into 64 subfaults, each 4 km long and 4 km wide. As an initial rupture model, we used uniform slip for all subfault elements. A comparison of the simulated and observed ground velocities for the uniform slip model is shown in the top panel of Figure 4. In general, this simple model matches the gross features of the observed responses (ie., timing and polarity), but it predicts waveforms which are too broad and it significantly underpredicts the peak amplitudes.

Using the uniform slip model as a starting point, we used an iterative trial and error modeling procedure to obtain our preferred variable-slip rupture model, which is displayed in Figure 5. The ground velocities computed for this model are compared with the observed records in the bottom panel of Figure 4. By using the variable-slip rupture model, we can produce ground motions which provide a very good match to the timing, waveform, and amplitude of most of the observed motions. A notable exception is the poor match to the vertical component recorded at station bunk. Unfortunately, the reliability of the long period signal in this trace may be somewhat questionable, since this time history was hand-digitized from an uncorrected analog recording having relatively small amplitude.

The variable-slip rupture model shown in Figure 5 is characterized by a concentrated region of large slip located near the hypocenter. Maximum slip values are about 8.5 m and the distribution of slip is consistent with rupture directivity to the southwest as reported by Ammon et al. (1993). A significant amount of slip must occur near the hypocenter, in order to match the absolute timing of the records at capm and petr. In addition, the short duration, simple pulses observed at these sites also indicate that most of the energy was released from a single asperity location. The northern portion of the fault plane has relatively low slip values (less than 2 m of displacement), although this is somewhat less well constrained due to the lack of absolute timing at station bunk. We have assumed that the large arrivals observed at bunk originated near the hypocenter.

## *Strong Motions in the Eel River Basin*

Figure 6 compares the ground velocities simulated using the variable-slip rupture model with the observed records at the five Eel River basin sites. Clearly, these synthetics provide a very poor match to the waveforms and amplitudes of the recorded data. By adjusting the near-surface structure of the plane-layered velocity model used in the FK simulation, we could potentially improve the fit to the amplitudes and horizontal/vertical partitioning of energy; however, a 1D velocity model is simply not capable of reproducing the large amplitude, late arrivals that are seen in the data. To match these features, we need to incorporate the 3D structure of the basin in our simulation process.

Much of information on the geology and structure of the Eel River basin has been summarized in the recent work by Clarke (1992). The structure of the basin is characterized by a thick sequence of Miocene and younger sediments overlying Franciscan Complex basement rock. Onshore, the thickness of the sediments reaches 3000 m, and the sequence extends to a thickness of 4000 m in the offshore regions. Cross-sections presented in the early work of Ogle (1953) provide constraints on the geometry of the onshore portion of the basin. Based on the information in these cross-sections, we have developed a 3D model of the Eel River basin.

Our primary region of interest is the portion of the basin surrounding the strong motion stations as shown in Figure 1. A detailed view of this region showing depth to basement contours is displayed in Figure 7. Due to the lack of specific information on the seismic properties of the sedimentary rocks, we have chosen velocities and densities for these units which are representative of their general classification. Although the surface velocity used in this model may be somewhat high ( $v_s = 1.0$  km/s), this unit represents an average of the media from the surface down to a minimum depth of 200 m.

In order to model the seismic response of the basin structure, we use a hybrid simulation technique which couples the far-field, analytic S-wave response of a finite-fault with a 3D elastic, staggered-grid finite-difference (FD) modeling algorithm (Graves, 1994). The model space used in the FD computations is 20 km wide, 20 km long, and extends to a depth of 5 km (see Figures 1 and 7). Using a grid spacing of 0.2 km, we obtain accurate results for frequencies up to 1 Hz in the lowest velocity regions of the model. We have also included  $Q$  in the FD calculation, using the technique presented in Graves (1994). Shear wave  $Q$  values of 40 and 80, respectively, were used for the two layers of basin sediments, and a value of 150 was used for the basement rock. The source used in this calculation is the variable-slip rupture model that was derived in the previous section.

Figure 8 displays profiles of synthetic ground velocities calculated using the 3D model of the basin structure for the six recording sites shown in Figure 7. The timing lines superimposed on these profiles are the same as those shown for the observed data in Figure 3. It is clear from this simulation that the large amplitude, late arrivals observed at the basin sites are related to the 3D response of the basin structure. We interpret these arrivals to be surface waves which are generated from the conversion of body wave energy at the southern margin of the basin. These surface waves propagate northward across the basin with relatively slow apparent velocity, leading to the long durations and large amplitudes that are seen in the ground motion recordings.

A more detailed comparison between the simulated and observed ground motions is shown in Figure 9. In general, the synthetic motions are in very good agreement with the amplitude,

waveform, and duration of the observed records. The poorest fit is at station bunk; however, since this site is very close to the fault plane (see Figure 1), the far-field source representation used in the simulation is probably not appropriate. For the horizontal components of motion, the synthetics are in excellent agreement with the response recorded at the basin sites. In both the synthetic and observed records, the basin generated surface waves are more dominant on the east-west component of motion than on the north-south component. Due to the relative geometry of the source location with the structure of the basin, and the general northward propagation of energy across the basin, we conclude that these surface waves are primarily comprised of horizontally polarized shear waves (SH energy). Our technique tends to overpredict the amplitude of the vertical component records, probably as a result of using a relatively high near-surface shear velocity ( $v_s = 1.0$  km/s).

In Figure 10, we map the ratios of the peak velocity and duration of the basin simulation to those obtained from a plane-layer FD simulation. For the plane-layer model, we have used the same velocity structure that was used in the calculation of the FK Green's functions given in Table 1. These figures demonstrate the relationship between the ground motion response of the basin sites and the relative geometry of the basin structure and the location of the earthquake source. In general, the relative peak velocity is highest within the basin sediments, although the distribution of these peak motions does not show a clear correlation with sediment thickness. In addition, while some sites within the central portion of the basin show large amplification factors (eg., near cent and fern), other sites, such as the area midway between fern and Iolt, show little or no amplification. This phenomenon results because ground motion levels are dependent not only on impedance contrasts, but also on wave propagation effects related to the focusing and defocusing of energy within the 3D structure of the basin. The lower panel of this figure shows that the relative durations generally increase northward across the basin. This results primarily from the northward propagation of surface waves, which are generated at the southern, near-source margin of the basin. One could easily envision that a source located to the north of the basin would create a significantly different pattern of ground motions, due to the southward propagation of surface waves across the basin. These types of effects do not occur in 1D structures.

## **Puget Basin Simulations**

Due to the lack of recorded strong motions for subduction events in the Puget Sound region, other means have been employed to derive estimates of expected ground motions for future large earthquakes. For example, empirical attenuation relations have been developed using data from other large subduction zone earthquakes (eg. Youngs et al., 1988; Crouse, 1991). However, using these relations to estimate ground motions in the Pacific Northwest requires the assumption that the source and wave propagation characteristics of the Cascadia region are similar to those of other subduction zones.

Several investigators have used simulation techniques to estimate expected ground motions from subduction zone earthquakes in this region of the Pacific Northwest (eg. Day et al., 1988; Heaton and Hartzell, 1989; Cohee et al., 1991; Wong et al., 1993; Youngs et al., 1993). These studies are expected to predict motions more specific to Cascadia than empirical estimates based on global data sets that do not include region-specific aspects of wave propagation. The scope

of the present work is to extend these types of simulation studies to longer periods and to address the issue of wave propagation effects through laterally varying basin structures.

There is clear evidence that the near surface structure in the Puget Sound region is strongly heterogeneous, being characterized by two deep sedimentary basins, separated by an east-west trending basement high (Figure 11). The basins are filled with unconsolidated glacial alluvium (Hall and Othberg, 1974; Yount et al., 1985) which creates a sharp impedance contrast with the underlying basement rocks.

Long-period ground motions can be simulated in the basin environments using the hybrid technique discussed in the previous section. As part of our first year's work, preliminary simulations have been performed in the Puget Sound region for a hypothetical  $M_w$  8 subduction zone event. We have used the fault model of Cohee et al. (1991), which is shown in Figure 12. The fault is divided into 25 subfault elements, each with dimensions of 30 km  $\times$  24 km. Weights are applied to each of the subfaults to model the effects of heterogeneous slip across the fault plane (Figure 13). For these simulations, we have modeled a 40 km  $\times$  40 km area of the Puget basin centered on the city of Seattle (Figure 14). The basin reaches its maximum depth of just over 1 km near downtown Seattle.

Figure 15 compares synthetic ground velocities computed using our hybrid modeling technique for a plane-layer velocity model with those obtained using the basin velocity model. These motions are for a site located on the southeast margin of the basin structure (see Figure 14). At very long periods (5-20 sec), the ground motions for both velocity structures are similar and are dominated by the earthquake source. However, at shorter periods (1-5 sec), the basin response shows much more complexity than the plane-layer response. These complex waveforms result from the trapping and focusing of 1-5 sec period energy within the basin structure. Due to the relatively shallow nature of the Puget basin, we expect that the ground motions in these structures will be most sensitive to these shorter periods. In addition, this suggests that the basin response will also be sensitive to source effects such as directivity, slip duration and rupture velocity, which are known to be important contributors to the ground motion response in this period range. These issues will be specifically addressed during the second and third years of this project.

## Conclusions

The 1992 Cape Mendocino earthquake is unique from other recent California earthquakes in that it appears to be a subduction type event associated with convergence along the Cascadia plate interface. The data recorded from this event provide us with a valuable opportunity to study source and wave propagation characteristics that are specific to the Cascadia Subduction Zone. By analyzing the ground motions produced during this event, we can begin to develop a framework for understanding and evaluating seismic hazards throughout the Pacific Northwest, as related to the Cascadia Subduction Zone.

Using constraints provided by the teleseismic focal mechanism and the distribution of aftershocks, we have developed a variable-slip rupture model of the Cape Medocino mainshock that explains the strong motion data recorded in the epicentral region. The fault model used in this study has nearly pure thrust motion on a shallow, eastwardly dipping fault plane. Our preferred slipmodel has a maximum displacement near 8.5 m, with most of the slip concentrated

in a small region near the hypocenter. This rupture model is representative of the deterministic ( $T > 1$  sec) features of the earthquake source.

Significant basin response effects are observed in the strong motion data recorded at sites located north of the epicentral region, in the Eel River basin. For these sites, large amplitude surface waves are prevalent at periods greater than 1 sec. These surface wave arrivals can be modeled using a hybrid simulation technique that accounts for source radiation from a finite-fault, as well as wave propagation effects through 3D geologic media. Our modeling indicates that the surface waves are generated from the conversion of source-radiated body waves at the southern margin of the basin. The surface wave energy propagates northward across the basin at a slow apparent velocity, leading to the large amplitudes and extended durations that are observed at the basin sites.

The simulation results presented in this study are very encouraging in that they demonstrate the utility of using numerical modeling techniques to understand source and wave propagation effects in regions of complicated geology. This is particularly important in areas such as the western portions of Oregon and Washington, which have a high seismic potential, but relatively few site-specific, ground motion recordings. By employing the simulation methods discussed in this paper, we can begin to address issues related to the quantification of expected levels of long-period ground motions for future events in these regions.

### Acknowledgments

This work was supported by USGS grant #1434-93-G-2327.

### References

- Ammon, C. J., A. A. Velasco, and T. Lay (1993). Rapid estimation of rupture directivity: Application to the 1992 Landers ( $M_s=7.4$ ) and Cape Mendocino ( $M_s=7.2$ ), California earthquakes, *Geophys. Res. Lett.*, **20**, 97-100.
- Clarke, S. H. (1992). Geology of the Eel River basin and adjacent region: Implications for late Cenozoic tectonics of the southern Cascadia Subduction Zone and Mendocino Triple Junction, *AAPG Bulletin*, **76**, 199-224.
- Cohee, B. P., P. G. Somerville, and N. A. Abrahamson (1991). Simulated ground motions for hypothesized  $M_w=8$  subduction earthquakes in Washington and Oregon, *Bull. Seism. Soc. Am.*, **81**, 28-96.
- Crouse, C. B. (1991). Ground motion attenuation equations for earthquakes on the Cascadia subduction zone, *Earthquake Spectra*, **7**, 201-236.
- Darragh, R., T. Cao, C. Cramer, M. Huang, and A. Shakal (1992). Processed CSMIP strong-motion data from the Cape Mendocino/Petrolia earthquake of April 25, 1992: release no. 1, CSMIP report OSMS 92-12.
- Day, S. M., J. L. Stevens, and T. G. Barker (1988). Ground motion simulations for thrust



- earthquakes beneath western Washington, Final report submitted to Washington Public Power Supply System, Richland, Washington.
- Graves, R. W. (1994). Simulating wave propagation in 3D elastic media using staggered-grid finite-differences, *manuscript in preparation*.
- Hall, J. B. and K. L. Othberg (1974). Thickness of unconsolidated sediments, Puget Lowland, Washington, State of Washington Department of Natural Resources, Geologic Map GM-12, Olympia, Washington.
- Hartzell, S.H. and T. Heaton (1983). Inversion of strong ground motion and teleseismic waveform data for the fault rupture history of the 1979 Imperial Valley, California, earthquake, *Bull. Seism. Soc. Am.*, **73**, 1553-1583.
- Heaton, T. H. (1990). Evidence for and implications of self-healing pulses of slip in earthquake rupture, *Phys. Earth Planet Interiors*, **64**, 1-20.
- Heaton, T. H. and S. H. Hartzell (1989). Estimation of strong ground motions for hypothetical earthquakes on the Cascadia subduction zone, Pacific Northwest, *Pure Appl. Geophys.*, **129**, 131-201.
- Mendoza, C. and S. H. Hartzell (1988). Aftershock patterns and main shock faulting, *Bull. Seism. Soc. Am.*, **61**, 1438-1449.
- Murray, M. H., G. A. Marshall, M. Lisowski, and R. S. Stein (1994). The 1992 Cape Mendocino, California, earthquake: A source model from geodetic data, *Seism. Res. Lett.*, **65**, p. 30.
- Ogle, B. A. (1953). Geology of the Eel River Valley area, Humboldt County, California, California Division of Mines and Geology, Bulletin 164, 128 p.
- Oppenheimer, D., G. Beroza, G. Carver, L. Dengler, J. Eaton, L. Gee, F. Gonzales, A. Jayko, W. H. Li, M. Lisowski, M. Magee, G. Marshall, M. Murray, R. McPerson, B. Romanowicz, K. Satake, R. Simpson, P. G. Somerville, R. Stein, and D. Valentine (1993). The Cape Mendocino, California earthquake sequence of April, 1992: Subduction at the triple junction, *Science*, **261**, 433-438.
- Saikia, C. K. (1993). Modified frequency-wavenumber algorithm for regional seismograms using Filon's quadrature - modeling of  $L_g$  waves in Eastern North America, *Geophysical J. Int.*, **118**, 142-158.
- USGS (1992). U. S. Geological Survey strong-motion records from the northern California (Petrolia) earthquake of April 25, 1992, USGS report, Menlo Park, California.
- Vidale, J. E., and D. V. Helmberger (1988). Elastic finite-difference modeling of the 1971 San

- Fernando, California earthquake, *Bull. Seism. Soc. Am.*, **78**, 122-141.
- Wald, D. J. and T. H. Heaton (1994). Spatial and temporal distribution of slip for the 1992 Landers, California, earthquake, *Bull. Seism. Soc. Am.*, **84**, 668-691.
- Wang, K. and G. C. Rogers (1994). An explanation for the double seismic layers north of the Mendocino triple junction, *Geophys. Res. Lett.*, **21**, 121-124.
- Wong, I. G., W. J. Silva, J. R. Humphrey, and I. P. Madin (1993). Site-specific ground motion estimates from a  $M_w$  8.5 Cascadia subduction zone earthquake for the Portland, Oregon metropolitan area, *Seism. Res. Letters*, **64**, Jan.-Mar. 1993.
- Youngs, R. R., S.-J. Chiou, W. J. Silva, and J. R. Humphrey (1993). Strong ground motion attenuation relationships for subduction zone earthquakes based on empirical data and numerical modeling, *Seism. Res. Letters*, **64**, Jan.-Mar. 1993.
- Youngs, R. R., S. M. Day and J. L. Stevens (1988). Near field ground motions on rock for large subduction earthquakes in *Proc. ASCE Conference on Earthquake Engineering and Soil Dynamics II: Recent Advances in Ground Motion Evaluation*, Geotechnical Special Publication 20, J. Lawrence von Thun (ed.), 445-462.
- Yount, J. C., G. R. Dembroff, and G. M. Barats (1985). Map showing depth to bedrock in the Seattle 30' by 60' quadrangle, Washington, U. S. Geological Survey Miscellaneous Field Investigations Map, MF-1692.

Table 1: Recent earthquakes in the Cape Mendocino region.

Date	hr:min:sec	Lat. (°N)	Lon. (°W)	Depth (km)	M <sub>s</sub>	M <sub>L</sub>
1/12/75	01:37:14.2	40.290	124.620	15	-	4.5
6/7/75	08:46:20.4	40.590	124.180	6	-	5.3
10/6/78	21:26:34.4	40.380	124.270	20	4.2	4.6
11/8/80	10:27:32.5	41.120	124.660	6	7.2	6.9
8/24/83	13:36:30.9	40.310	124.770	30	5.8	5.5
4/25/92	18:06:05.2	40.327	124.229	10	7.1	-

Table 2: Velocity model for Cape Mendocino region.

$V_p$ (km/s)	$V_s$ (km/s)	$\rho$ (g/cc)	$Q_p$	$Q_s$	Th (km)
3.0	1.5	1.5	200	100	0.2
4.6	2.3	1.8	300	150	4.8
5.6	3.2	2.3	500	230	9.5
6.8	3.9	2.8	600	270	15.5
8.1	4.7	3.3	1000	500	-

## Figure Captions

**Figure 1:** Map showing locations of USGS and CSMIP strong motion recording sites in the Cape Mendocino region. Small stars indicate locations of previous events recorded in this region. Large star and rectangular shaded region indicate the epicenter and rupture area, respectively, of the 1992 event. The hatched region to the north of the rupture area delineates the Quaternary sediments of the Eel River basin, where several of the strong motion sites are located. The box enclosing these sites depicts the areal extent of the finite-difference model space used in the numerical simulations.

**Figure 2:** Ground velocities (integrated from recorded accelerations) for the sites shown in Figure 1. These motions have been bandpass filtered in the period range of 1-7 sec.

**Figure 3:** Three-component profiles of filtered ground velocity for the Eel River basin sites. The traces are plotted as a function of increasing epicentral distance. Superimposed on these profiles are timing lines indicating the approximate arrival of the direct S-wave (dashed line) and a later set of arrivals, which are thought to be basin generated surface waves (solid line).

**Figure 4:** Comparison of ground velocities observed at the three near-fault strong motion sites for the Cape Mendocino earthquake with results simulated using a uniform-slip rupture model (top panel) and those simulated using a variable-slip rupture model (bottom panel). Both data and synthetics have been low-pass filtered at 1 Hz.

**Figure 5:** Preferred rupture model of the Cape Mendocino earthquake determined from deterministic modeling. The top panel shows final slip values for each of the subfault elements with the hypocenter location indicated by the star. The bottom panel indicates the direction of slip (rake) across the fault plane. The length of the slip vectors are scaled to the final slip values.

**Figure 6:** Comparison of ground velocities observed at sites to the north of the fault plane in the Eel River basin, with synthetics computed for the preferred rupture model using a plane-layered velocity structure.

**Figure 7:** Map showing depth to basement rock in the vicinity of the Eel River basin. The region shown corresponds to the areal extent of the model space used in the finite-difference simulations (see Figure 1).

**Figure 8:** Three-component profiles of ground velocity computed for the Eel River basin sites using the hybrid FD simulation technique with the basin model shown in Figure 7. The traces are plotted as a function of increasing epicentral distance. Superimposed on these profiles are the same timing lines that are shown in Figure 3.

**Figure 9:** Detailed comparison of observed and simulated ground velocities for the Eel River basin sites. For each pair of traces, the top trace is the data and the bottom trace is the synthetic response calculated for the 3D basin model. Each pair of traces is normalized to the same

amplitude.

**Figure 10:** Relative peak velocity (top) and relative duration (bottom) for the 3D Eel River basin simulation compared with a plane-layer velocity model simulation.

**Figure 11:** Map view showing depth to basement rock in the Puget Sound region, near the cities of Seattle and Tacoma.

**Figure 12:** Fault model and geometry for a hypothetical  $M_w$  8 subduction zone event on the Cascadia plate interface in the Puget Sound region.

**Figure 13:** Prescribed slip model for the hypothetical  $M_w$  8 earthquake.

**Figure 14:** 3D structural model for the Puget basin near the city of Seattle which is used in the simulation of the hypothetical event.

**Figure 15:** Simulation results for a site in the city of Seattle for the case of plane-layered structure and 3D basin structure. The top panels show the response in the period range 5-20 sec and the bottom panels show the response in the period range 1-5 sec.

Figure 1

# Cape Mendocino Earthquakes

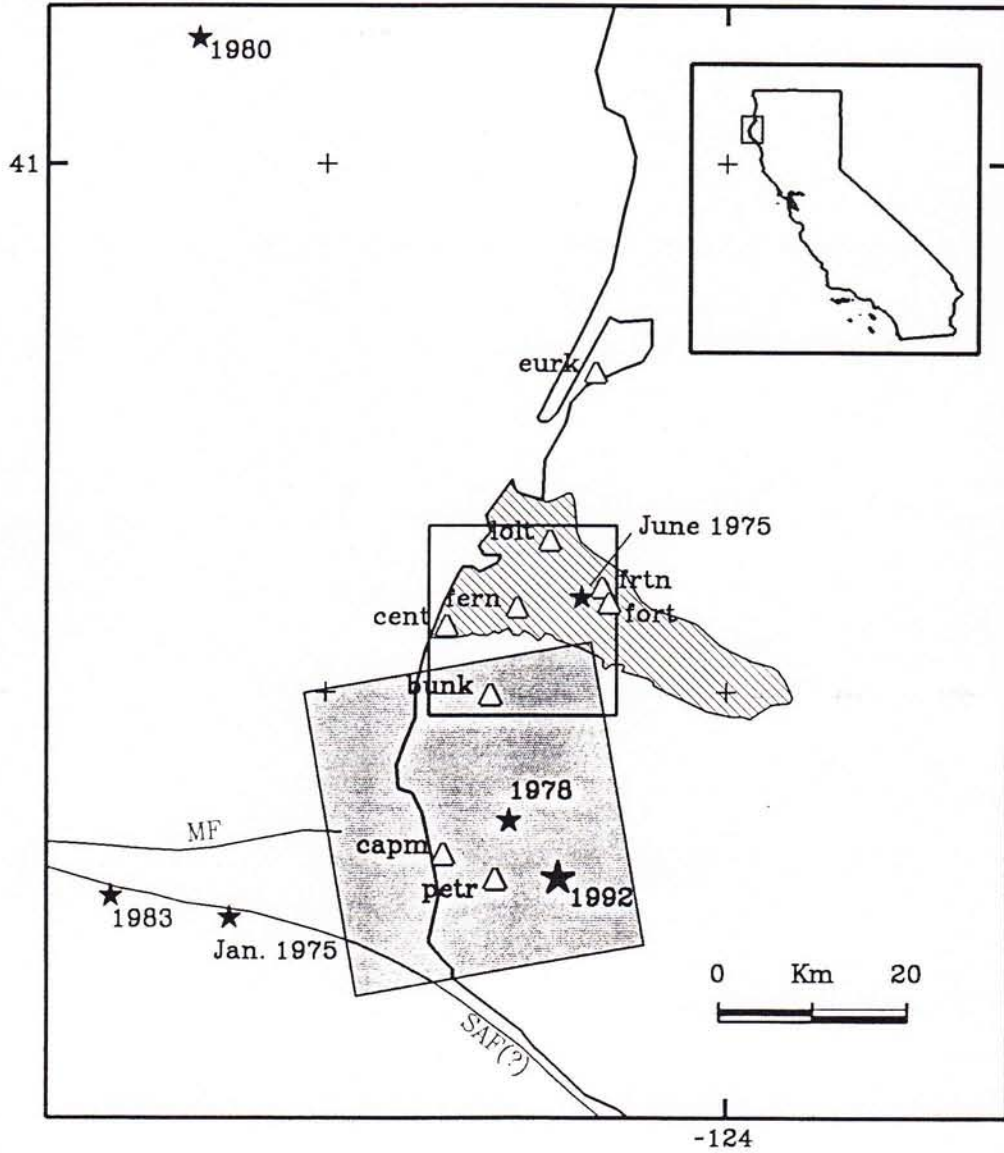


Figure 2

# Cape Mendocino EQ

Velocity Recordings, Low-pass at 1 Hz

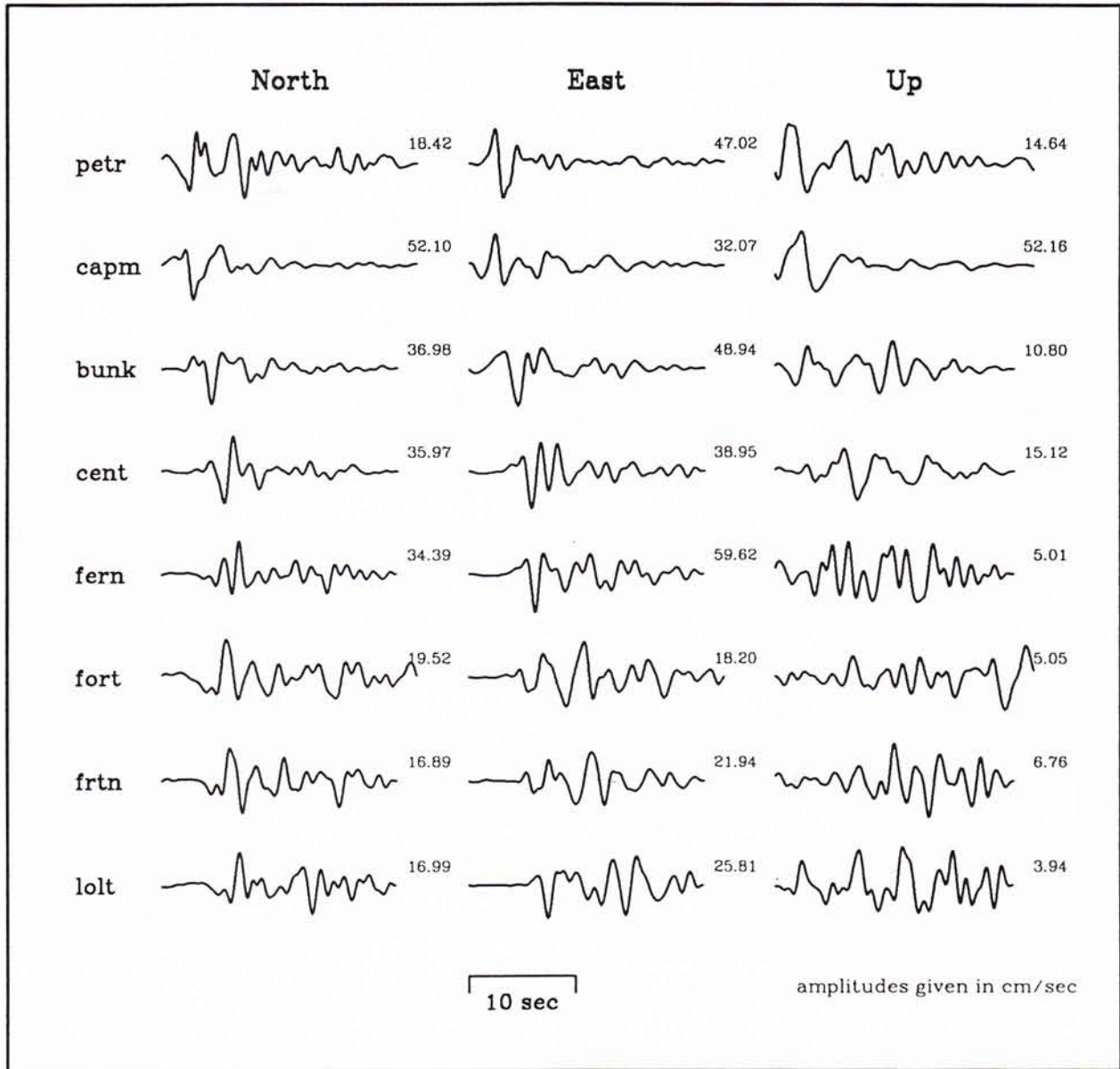




Figure 3

# Cape Mendocino EQ

## Velocity Recordings: Eel River Basin Sites

*Low-pass at 1 Hz*

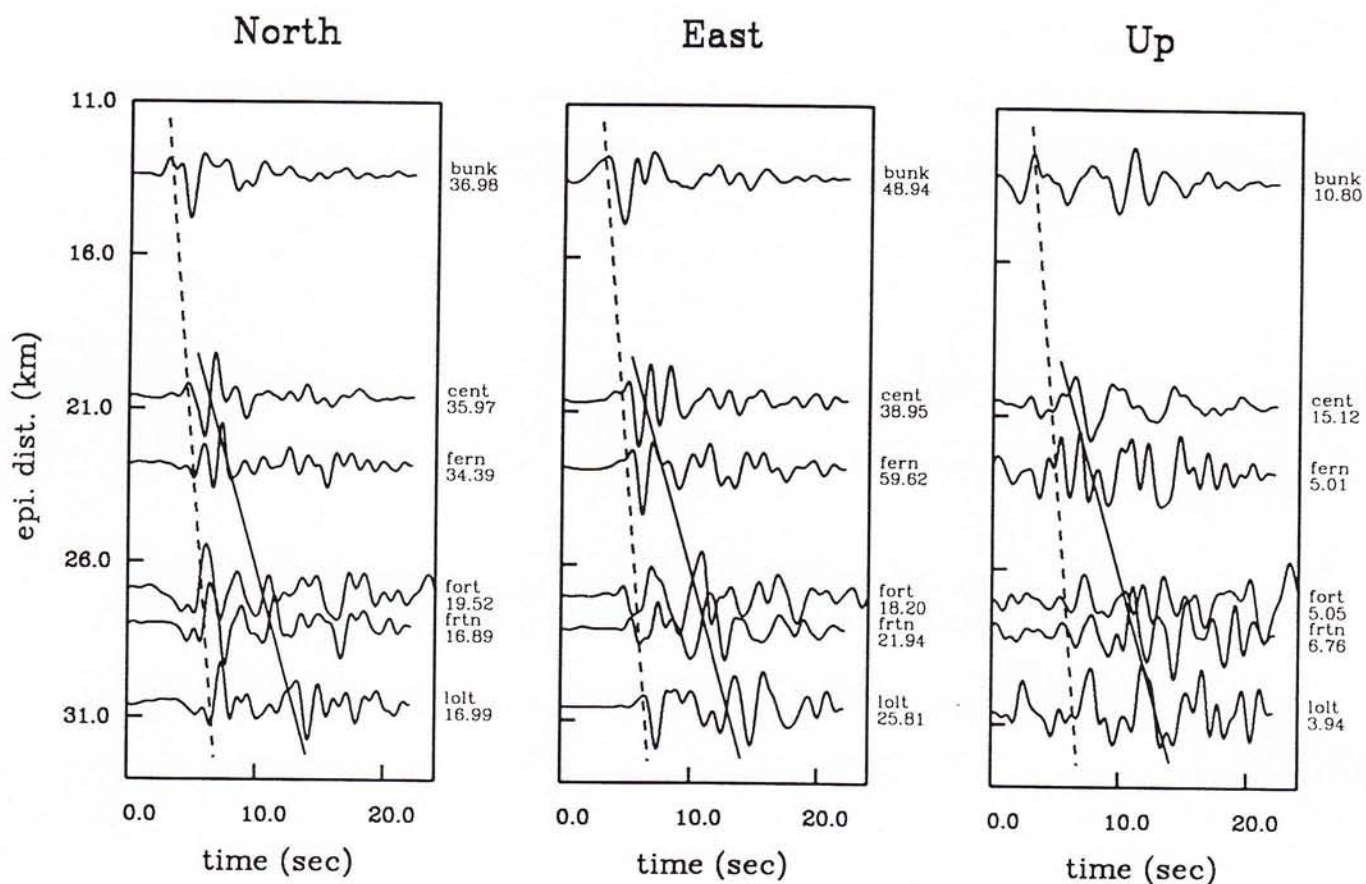
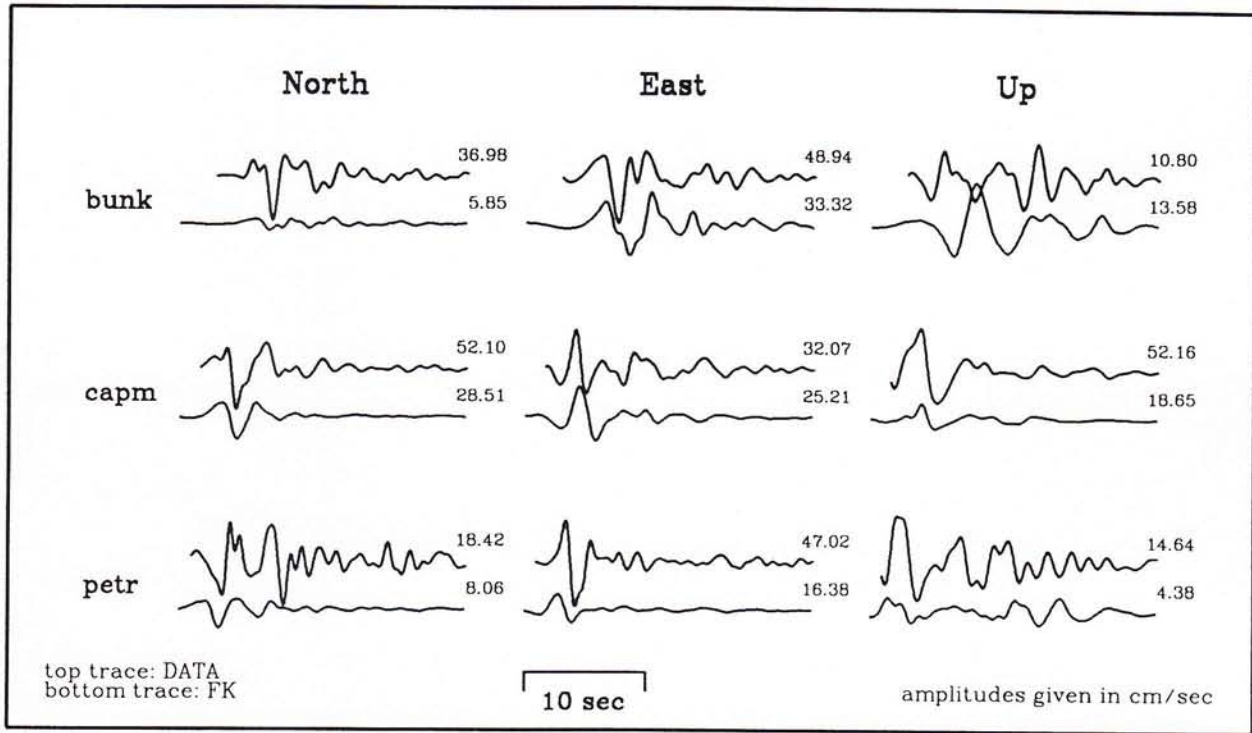


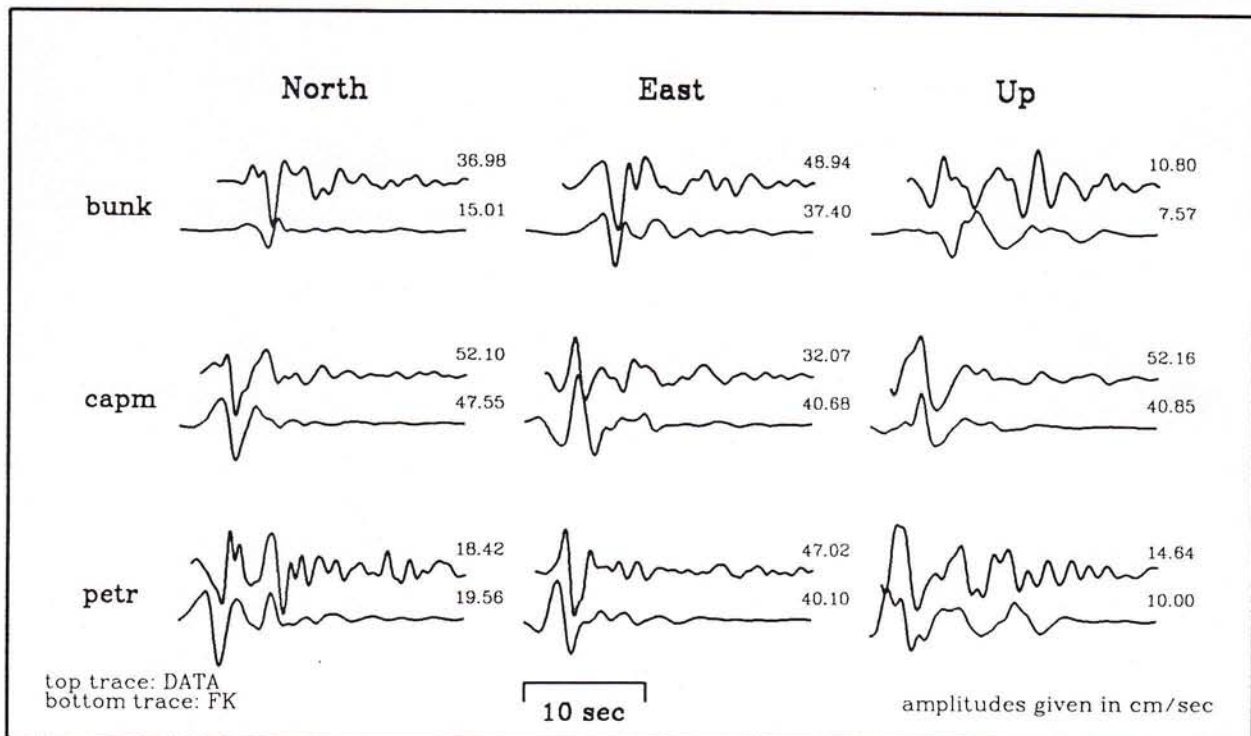
Figure 4

# FK Simulation: Cape Mendocino

## Uniform Slip



## Variable Slip



# Cape Mendocino Slipmodel

strike = 350°  
dip = 14°  
rake = 105°  
moment = 3.0e+26 dyne-cm

length = 32 km  
width = 32 km  
depth to top = 4.2 km  
Mw = 7.0

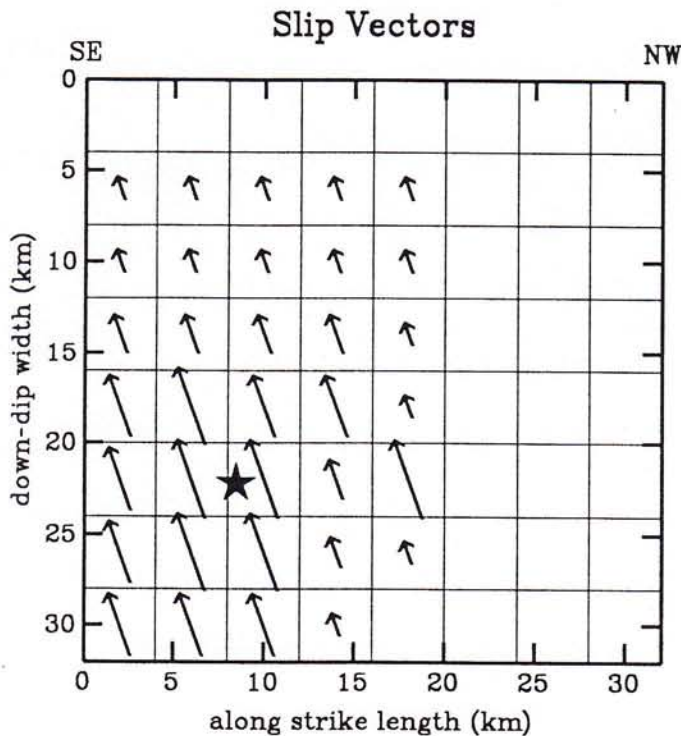
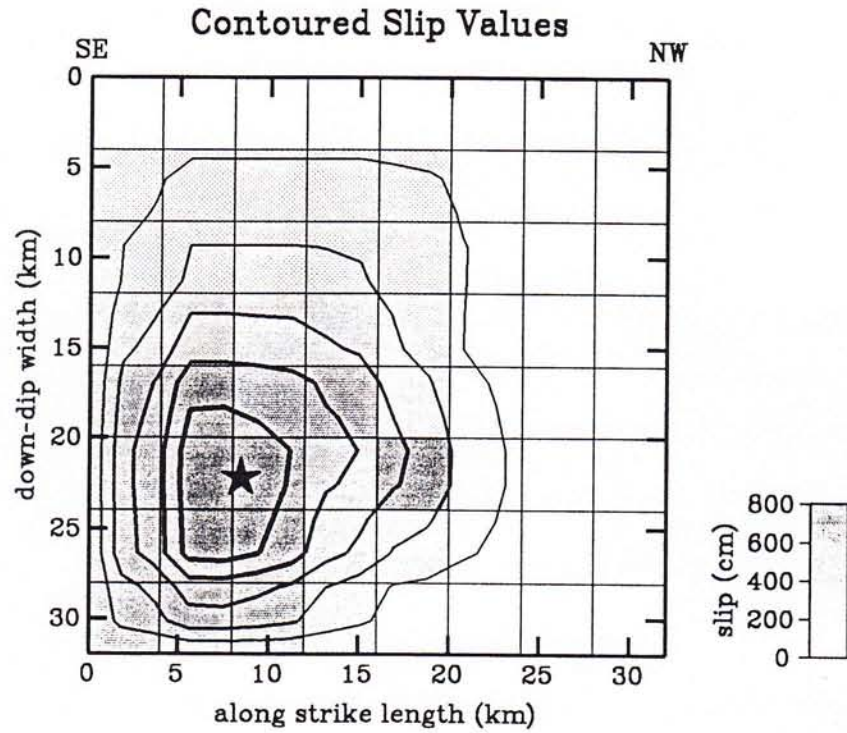


Figure 6

# FK Simulation: Cape Mendocino

Velocity Model M4, Variable slip

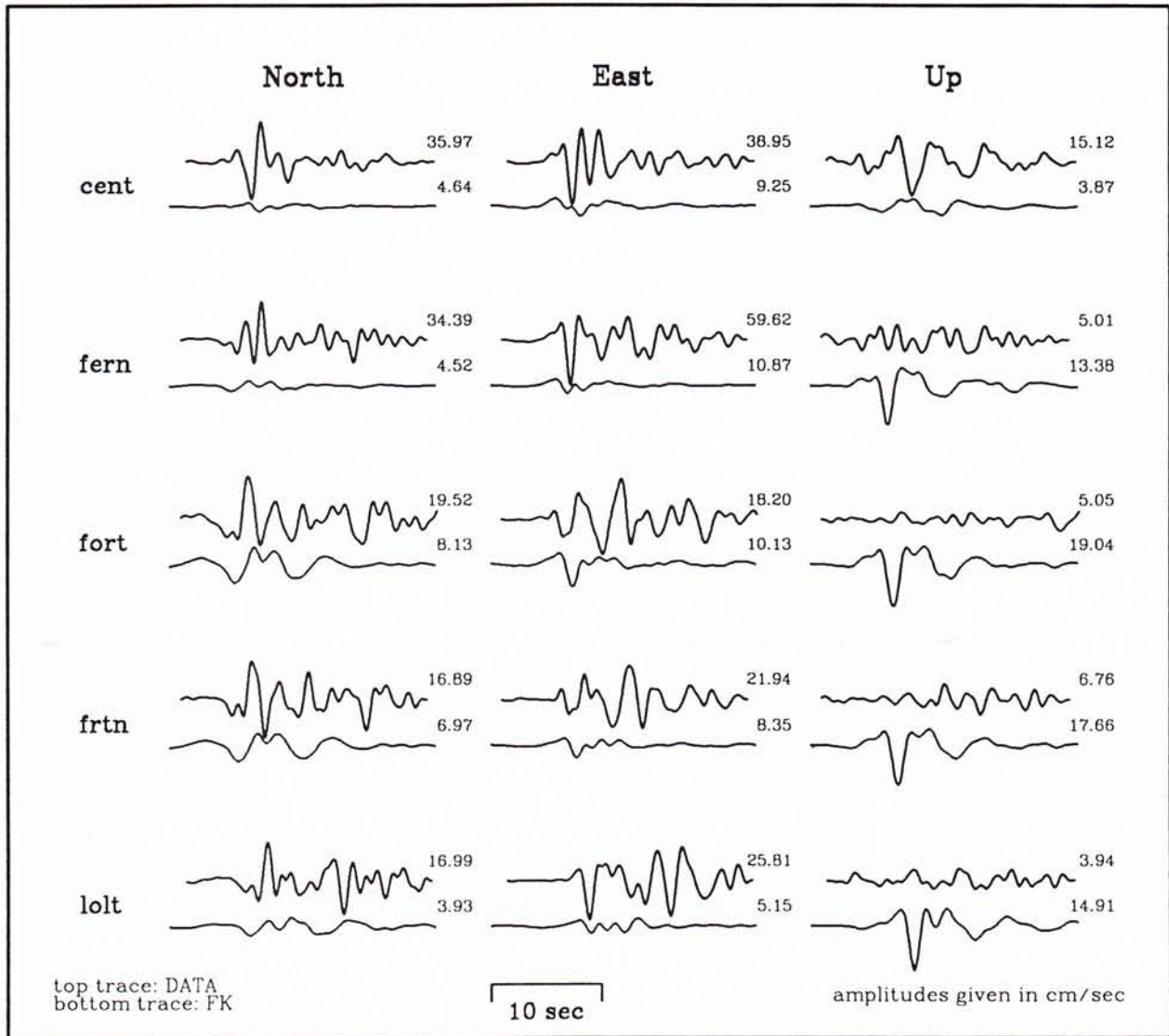
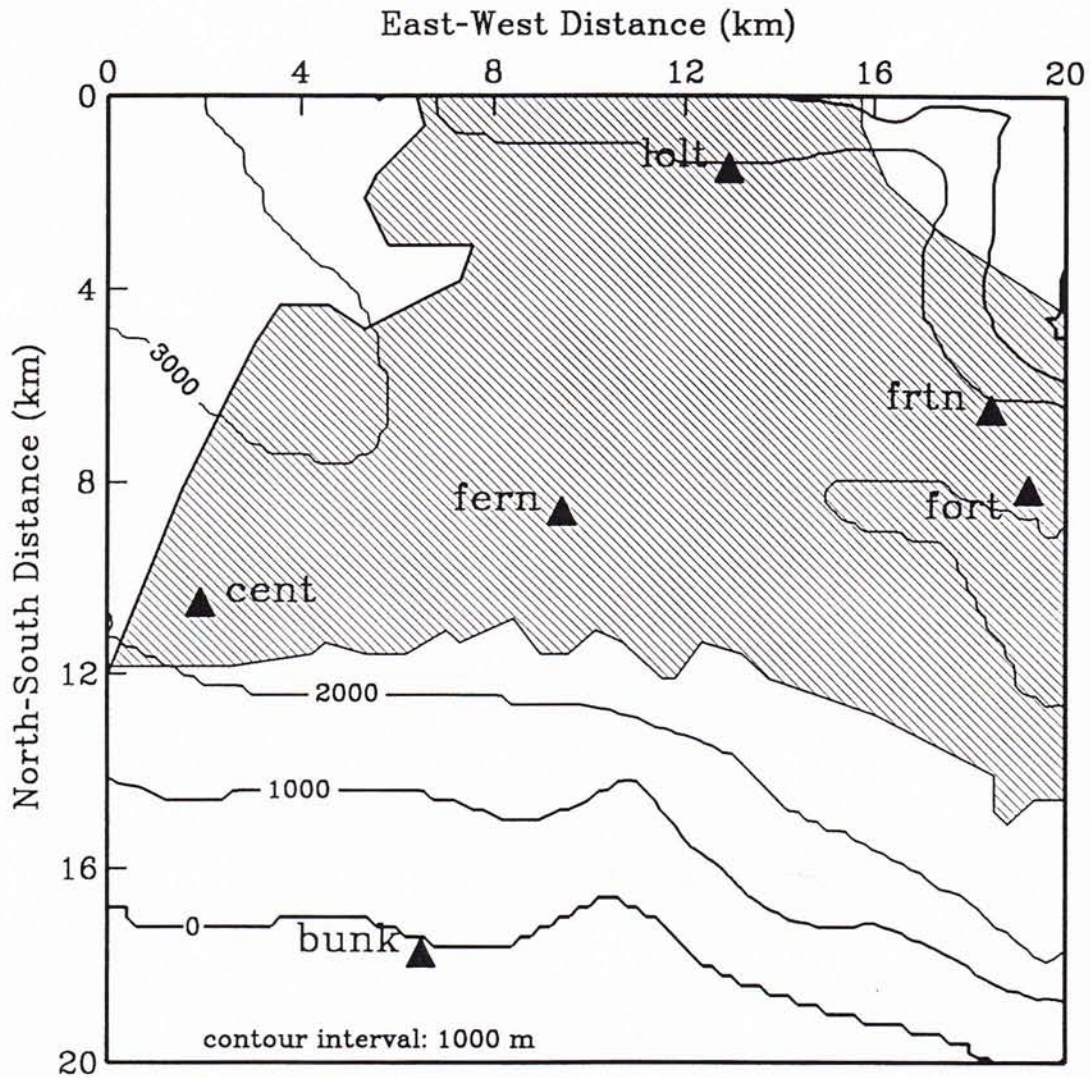
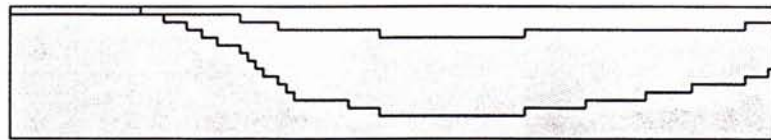





Figure 7

# Eel River Basin Model



south-north cross-section at fern



-   $\alpha = 2.000 \text{ km/sec}$   
 $\beta = 1.000 \text{ km/sec}$   
 $\rho = 1.4 \text{ g/cc}$
-   $\alpha = 2.800 \text{ km/sec}$   
 $\beta = 1.500 \text{ km/sec}$   
 $\rho = 1.7 \text{ g/cc}$
-   $\alpha = 4.600 \text{ km/sec}$   
 $\beta = 2.300 \text{ km/sec}$   
 $\rho = 1.8 \text{ g/cc}$

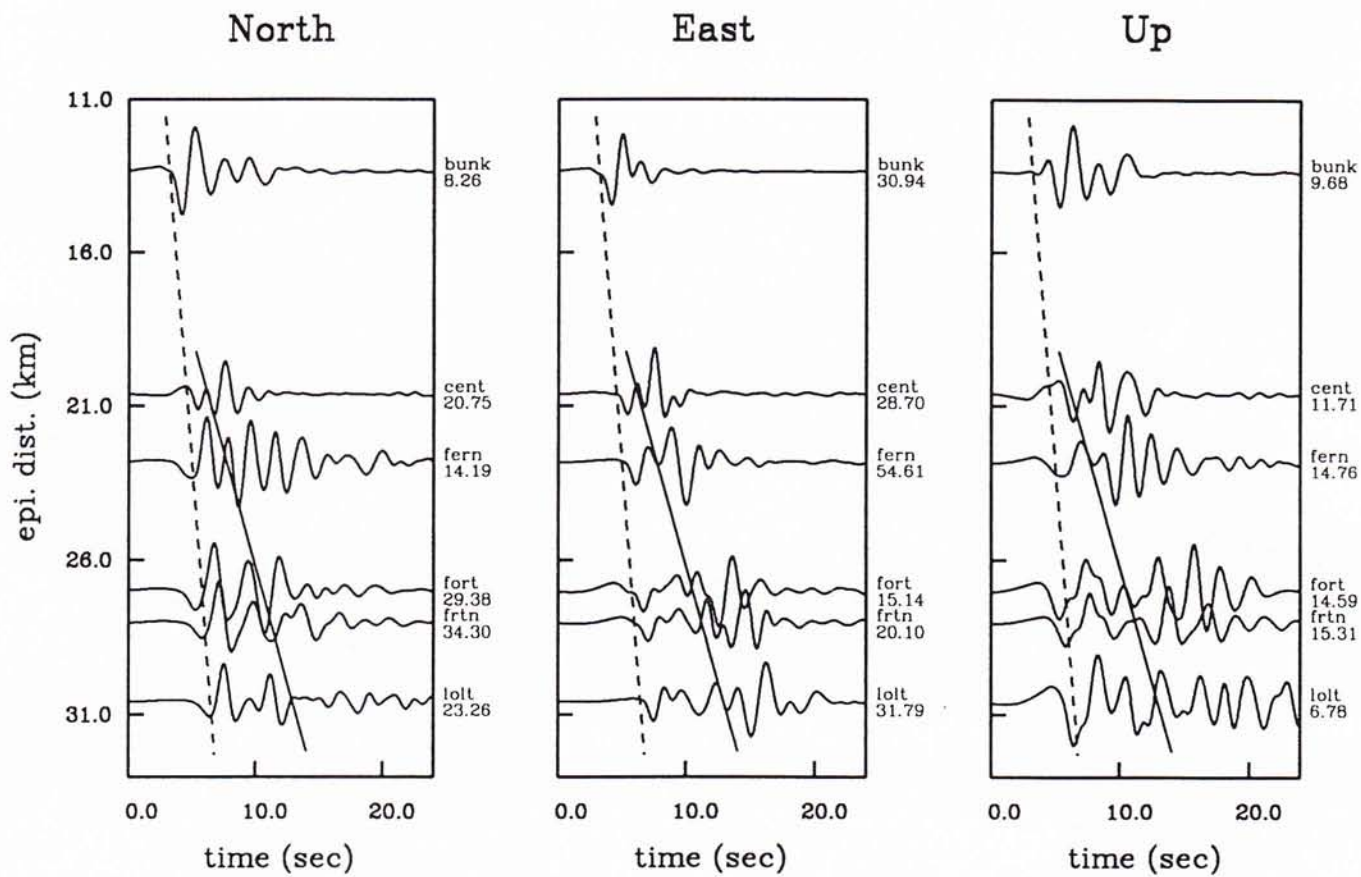
horizontal scale

0 km 5.0

# Cape Mendocino EQ

## 3D FD Simulation: Eel River Basin Sites

*Low-pass at 1 Hz*



# FD Simulation: Cape Mendocino

Basin Model, Variable slip, with Q

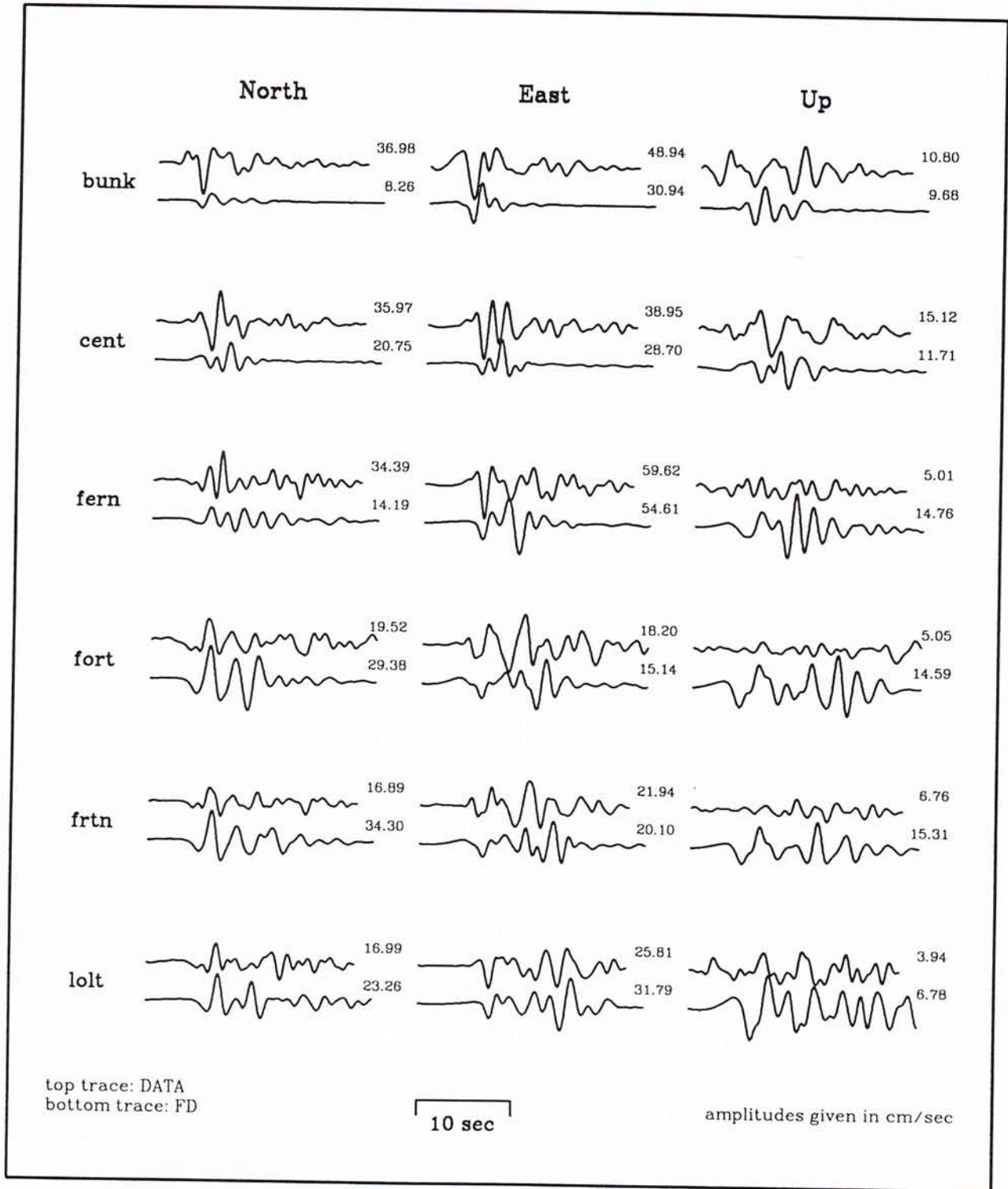
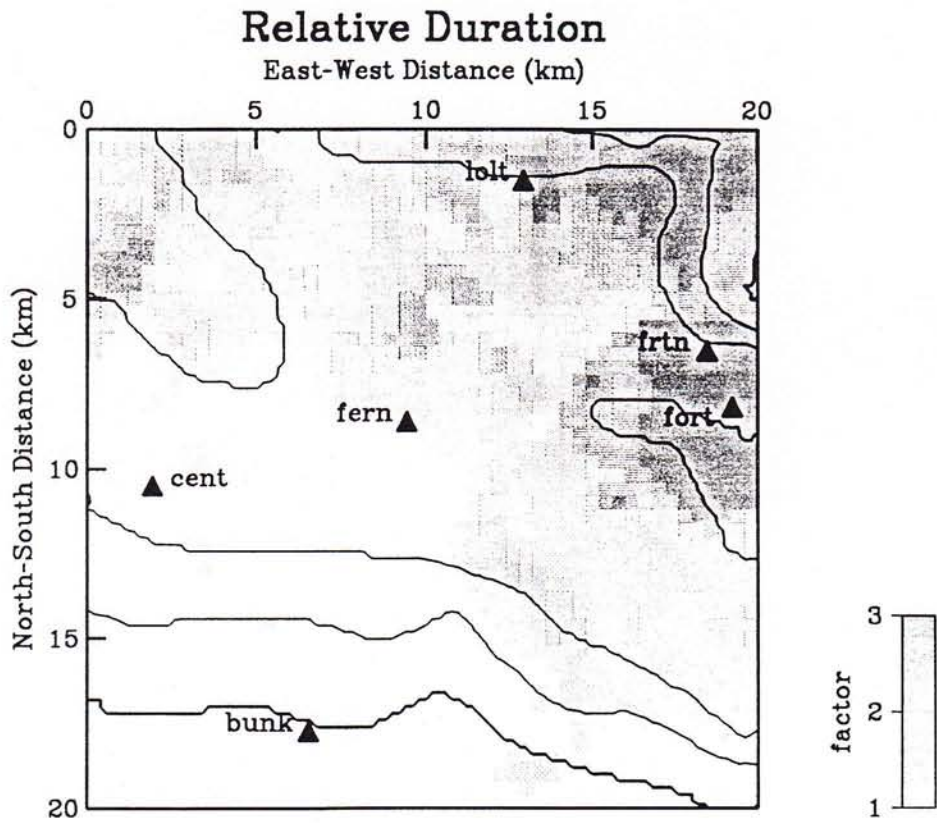
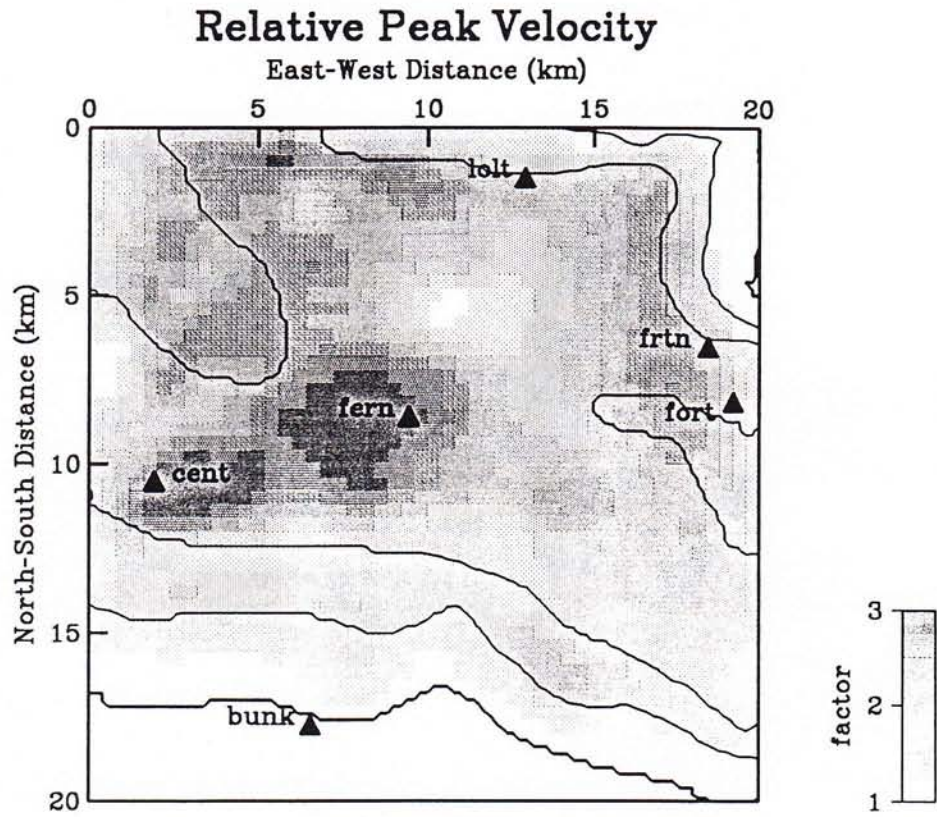


Figure .10





# Puget Sound Basin Model

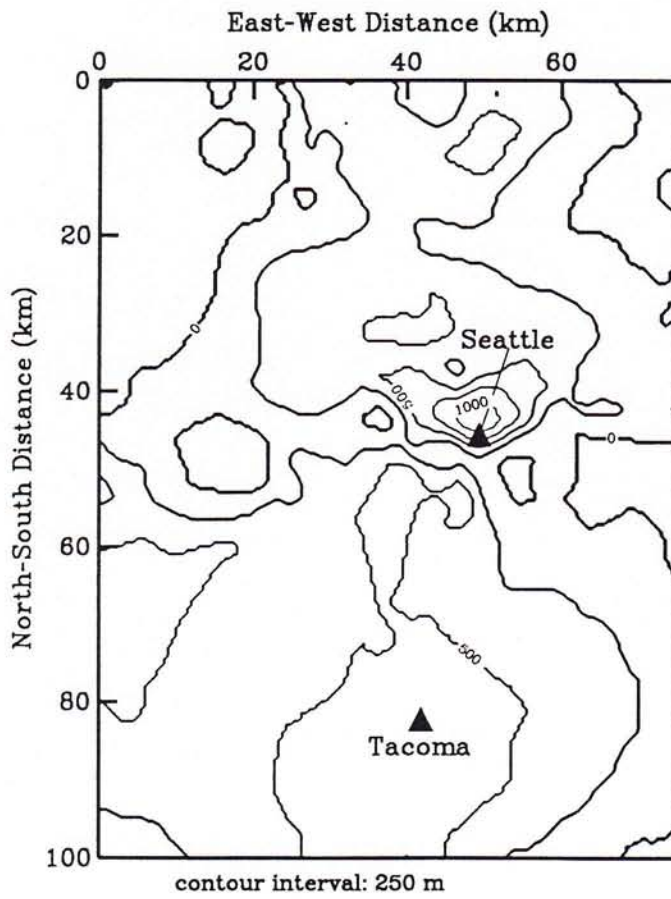
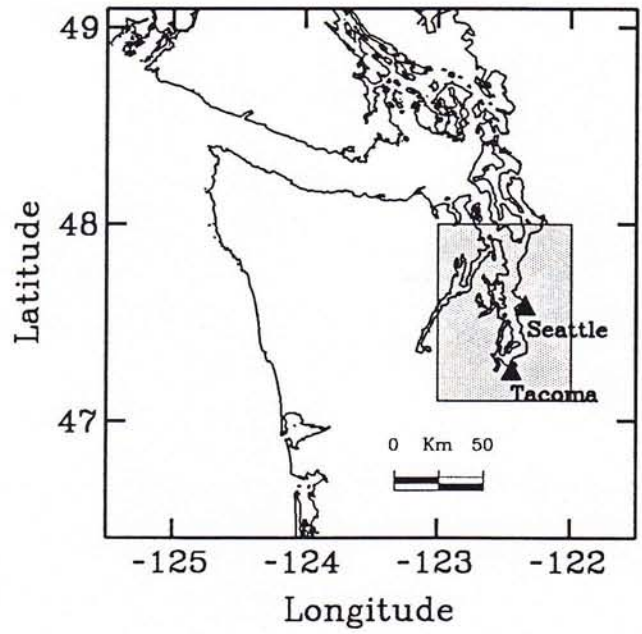


Figure 12

# Puget Sound Fault Model

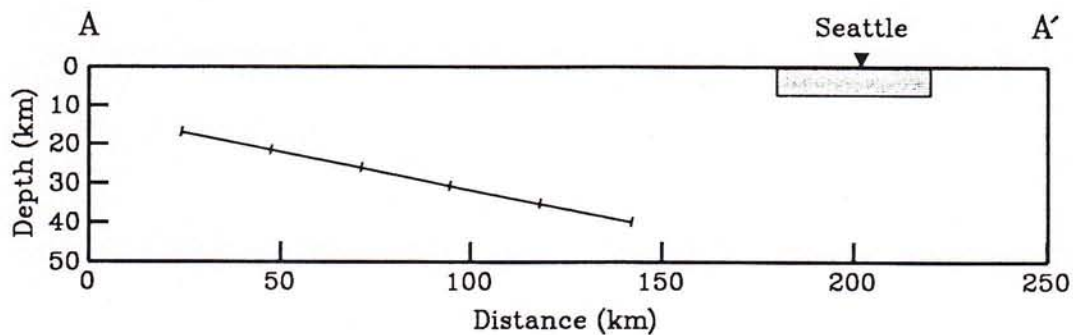
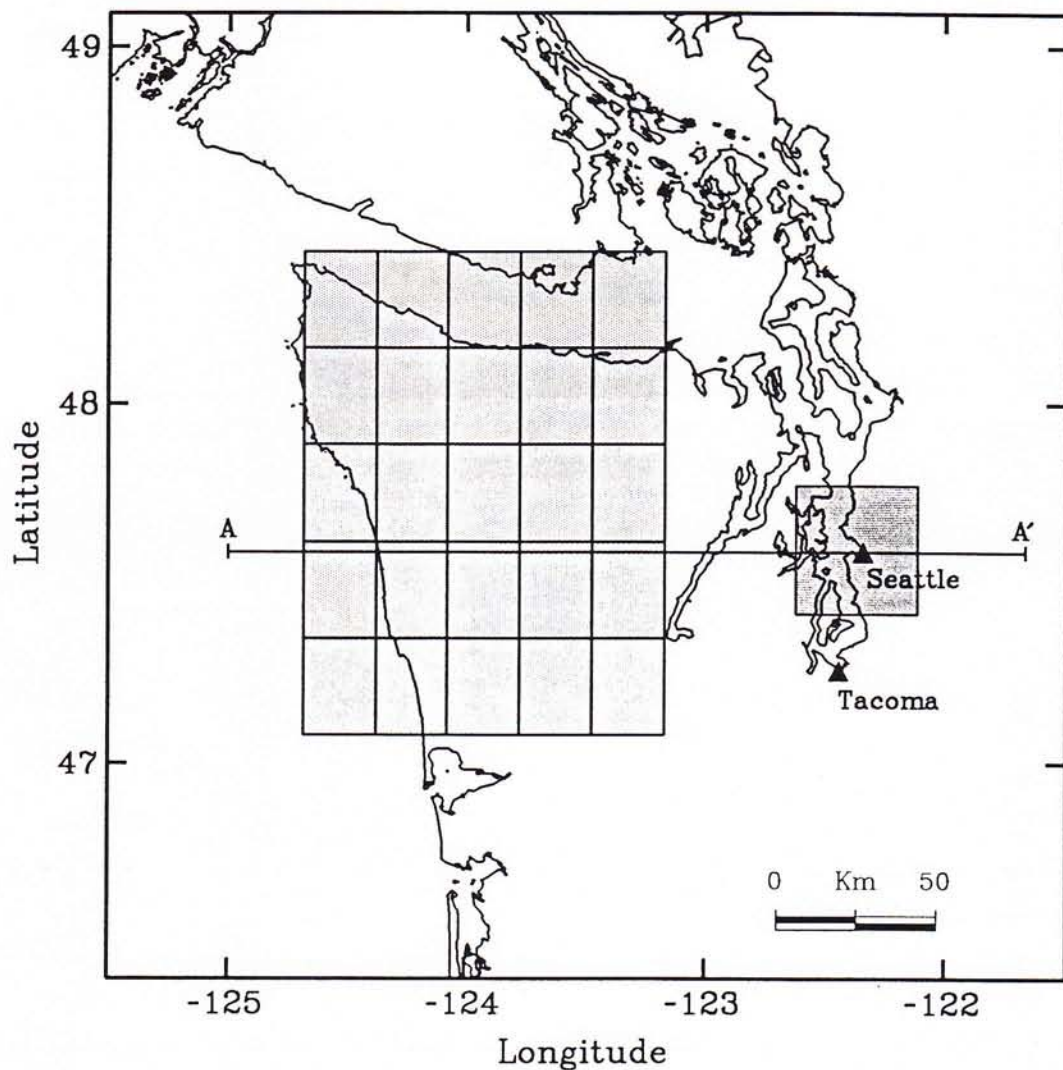
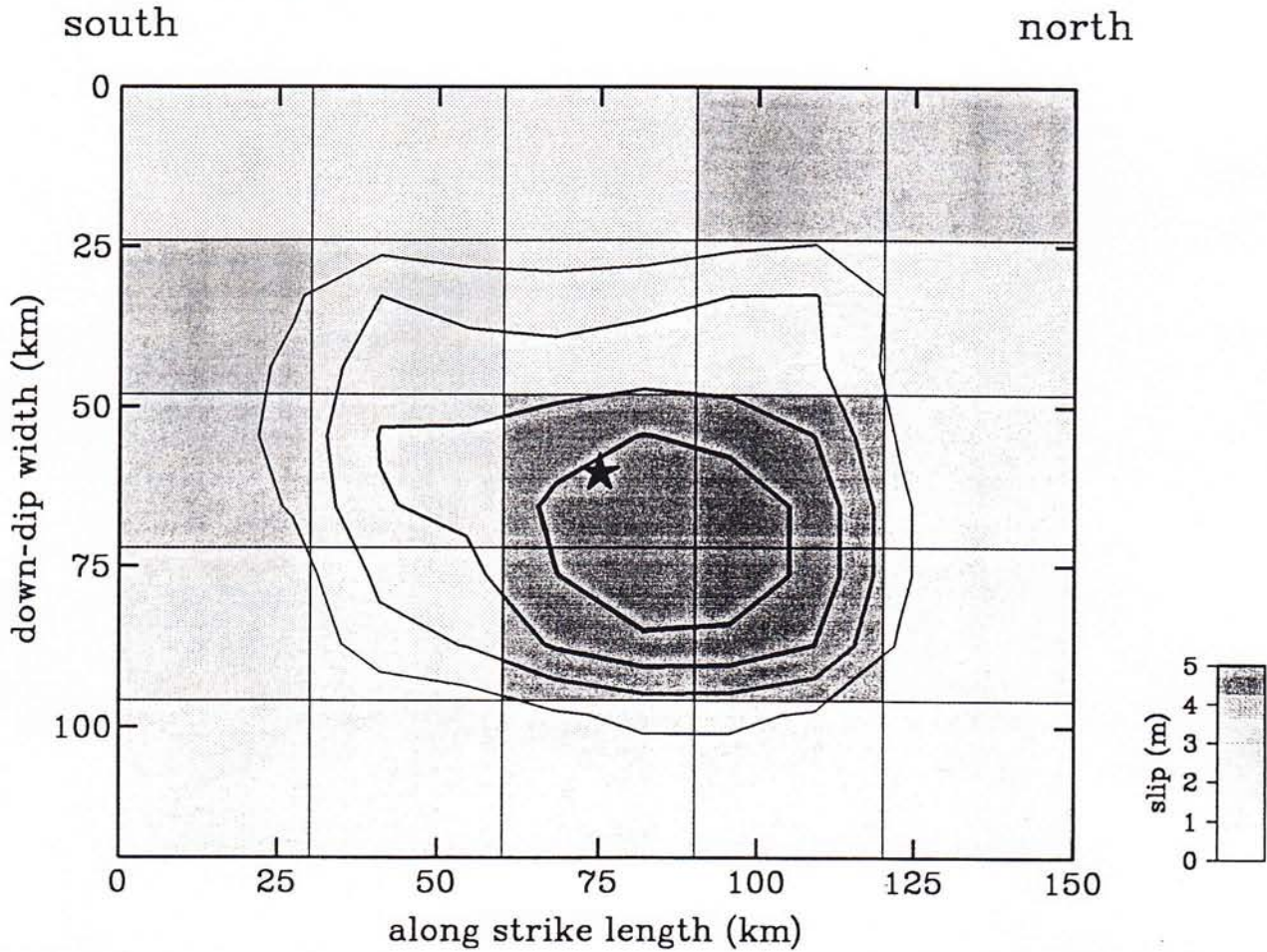


Figure 13

## Puget Sound Slipmodel: Mw 8



strike =  $0^\circ$

dip =  $11^\circ$

rake =  $90^\circ$

moment =  $1.12e+28$  dyne-cm

length = 150 km

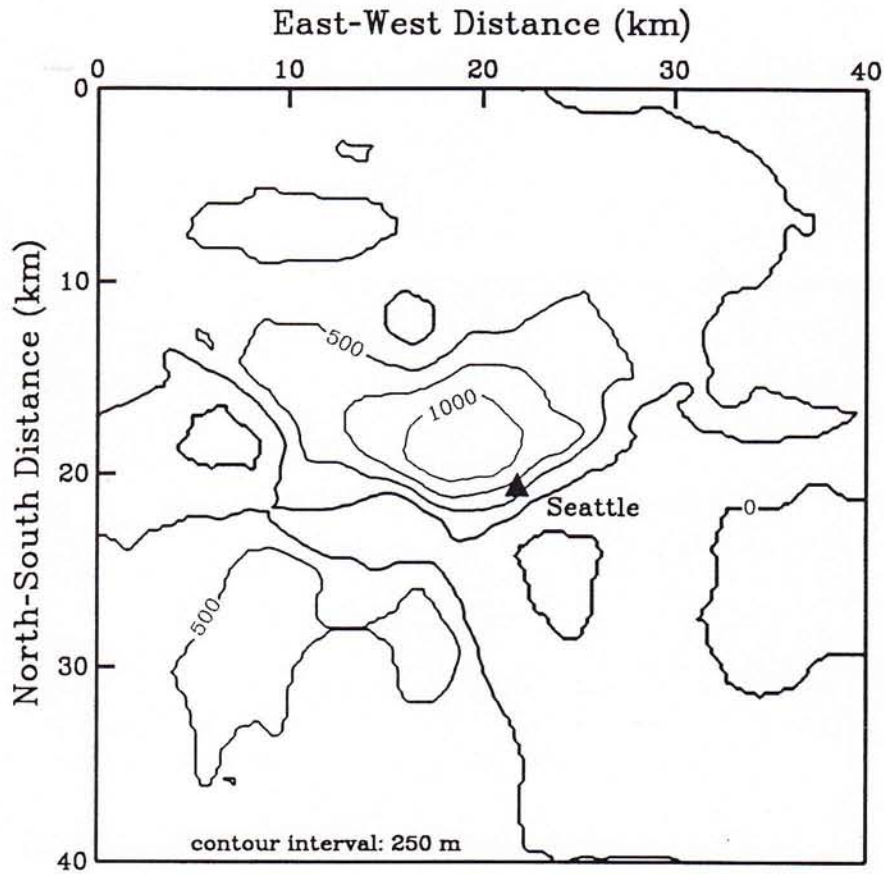
width = 120 km

depth to top = 17 km

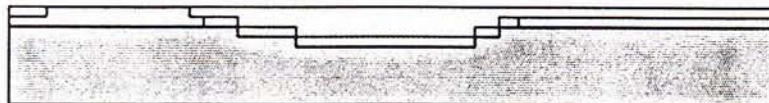
Mw = 8.0

Figure 14



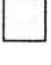

# Puget Basin Model



west-east cross-section at NS=18km



vertical exaggeration 2:1

-   $\alpha = 2.000 \text{ km/sec}$   
 $\beta = 1.000 \text{ km/sec}$   
 $\rho = 1.4 \text{ g/cc}$
-   $\alpha = 2.800 \text{ km/sec}$   
 $\beta = 1.500 \text{ km/sec}$   
 $\rho = 1.7 \text{ g/cc}$
-   $\alpha = 3.000 \text{ km/sec}$   
 $\beta = 1.500 \text{ km/sec}$   
 $\rho = 1.5 \text{ g/cc}$
-   $\alpha = 4.600 \text{ km/sec}$   
 $\beta = 2.300 \text{ km/sec}$   
 $\rho = 1.8 \text{ g/cc}$

horizontal scale  
0 km 10.0

# Puget Basin Response: Seattle

